Materials Research Proceedings 28 (2023) 1861-1870 https://doi.org/10.21741/9781644902479-201

Effect of compression during post-treatment to improve the mechanical strength of printed carbon fiber/ PEKK composites

COMBETTES Julien[1,a *], ABADIE Amandine[1,b], FAZZINI Marina[1,c], BORLENGHI Andrea[2,d], BOSSHARD Jonas[2,e], GARNIER Christian[1,f], DESSEIN Gilles[1,g] and CHABERT France[1,h]

[1]LGP-ENIT-INPT, University of Toulouse, 47 Avenue d'Azereix, BP1629-65016 Tarbes Cedex, France

[2]9TLabs, Badenerstrasse 790, 8048 Zürich, Switzerland

[a]jcombett@enit.fr, [b]amandine.abadie@enit.fr, [c]marina.fazzini@enit.fr, [d]andrea@9tlabs.com, [e]jonas@9tlabs.com, [f]christian.garnier@enit.fr, [g]gilles.dessein@enit.fr, [h]france.chabert@enit.fr

Keywords: Additive Manufacturing, Carbon Fiber, Composite, Porosity, Post-Treatment

Abstract. This work aims to understand the effect of consolidation on parts obtained by material-extrusion additive manufacturing process. Three plates were manufactured with carbon fiber/PEKK tapes. Two of them were consolidated under pressure at 334 and 360°C corresponding to the maximum of the melting peak and the end of the melting peak of PEKK respectively. Another plate did not undergo any post-treatment after printing, it is used as a reference. The parts were characterized to measure their porosity by density measurement and X-ray micro-computed tomography. Subsequently, short beam shear tests and dynamic mechanical analysis (DMA) tests were carried out to assess the influence of porosity on the mechanical strength of the plates. As expected, the interlaminar shear strength (ILSS) decreases when the porosity increases. The highest ILSS is obtained for the part consolidated at 360°C due to a lower porosity. The highest storage modulus is obtained for the part consolidated at 334°C whereas the loss factor indicates a lower glass transition for the same part. This could be explained by a lower degree of crystallinity as revealed by DSC, compared to the part consolidated at 360°C.

Introduction

Additive manufacturing offers affordable opportunity to obtain complex shapes [1]. Material-extrusion based processes are the most used techniques of 3D printing. ASTM International's additive manufacturing (AM) technologies committee approved a new standard guide for the use of layer-based material extrusion (MEX) processes in additive manufacturing. MEX processes are used to fabricate polymer, or polymer composite, parts by depositing a filament or bead of material from an extrusion head. Initially, most of raw materials were filaments of polylactic acid (PLA) and acrylonitrile butadiene styrene (ABS). Indeed, because of their low thermal transitions, their printing temperatures fit any basic printing machine [2,3]. However, after printing, such printed parts often suffer from poor interlayer adhesion bonding and high porosity rate [4]. MEX is now driven by high demanding applications, which require high performance polymers. PEEK (polyetheretherketone) and PEKK (polyetherketoneketone) are high performance semi-crystalline thermoplastics whose glass transition and melting temperatures are around, respectively, 150°C and above 360°C [5,6]. Printing PEEK and PEKK is possible with machines equipped with a heating chamber to control the crystallization upon cooling. As shown by Wang et al. [7] who characterized the bending properties of PEEK, printed parts reached 190 MPa for the bending strength compared to around 200 to 300 MPa for an injection molded part [8]. Other works report similar trends regarding mechanical resistance for PEKK printed parts [9]. Indeed, printing of PEKK is a challenge due to its high deposition temperature of around 400°C and its very high viscosity. Such high temperatures induce harsh temperature gradients inside the part during

printing. Consequently, the crystallization of PEKK is not homogeneous along the z-axis direction. This gradient of crystallinity contributes to warpage defects due to anisotropic shrinkage. Also, a too fast crystallization could hinder macromolecular diffusion at the interfaces, the surface contact between filaments. Thus, the mechanical resistance between each layer of PEEK or PEKK printed parts remains very low as demonstrated by Rahman et al. who measure an interlayer resistance between 80 and 100 MPa [10]. A way to improve the mechanical properties of thermoplastics is the association with short or continuous fibers. Among fibers, carbon fibers have the highest elastic modulus and stress at break. Therefore, some studies have focused on printing carbon fiber/polyetherketoneketone (PEKK) composites which target aerospace, medical and any other demanding applications due to outstanding chemical resistance, flame retardancy and low smoke generation and toxicity [11]. When filled with short carbon fibers (100 to 300 μm), the performance of these composites is limited [12,13] as revealed by their brittle behavior under impact [14], but the short fibers increases the tensile strength up to 95 MPa against 80 MPa for the pure PEEK [15]. Addition of continuous fibers makes the material much more resistant [15]. The stiffness, low weight and stress resistance make continuous carbon fiber an ideal material to produce industry-grade composite parts. Unfortunately, long carbon fiber/PEEK printed parts also suffer from high porosity and poor interlayer adhesion as demonstrated by Luo et al. who found an interlaminar shear strength (ILSS) of 4 MPa for a 20%wt long carbon fiber filled composite, compared to an ILSS of 12 MPa when printing pure PEEK [16]. An option to overcome this flaw has been put forward by Van de Werken et al. who studied the effect of hot-pressing as post-treatment after printing. After applying a temperature of 250°C for less than 3 hours at 1.4 MPa, the porosity was decreases by a factor 2 to achieve 5% of porosity with an ILSS of 35 MPa [17].
9Tlabs is a company offering solutions to design and manufacture complex parts in no time. They propose additive manufacturing machines to produce high performance continuous fiber composites (carbon fiber with PEEK or PEKK matrix) with up to 60% fiber volume fraction. High volumes of structural composites can be manufactured in achieving up to 80% weight saving and 50% cost saving in series production, high reproducibility and great quality [18]. Their solution is based on a two step process: 1) a printing step 2) a consolidation step.

In this article, the effect of the consolidation step on the part performance was evaluated. The porosity rate and mechanical properties of the parts were measured on printed parts and after consolidation step at two different temperatures at 334°C and 360°C. The porosity was measured by density measurement and micro-computed tomography (μCT). The benefits and limitations of these techniques are discussed. The mechanical strength of printed parts was measured by interlaminar shear strength (ILSS). The material moduli were determined by dynamic mechanical analysis (DMA). An attempt to correlate these results to the porosity of parts is proposed to highlight the effect of compression post-treatment.

Materials

The composites plates were manufactured with a 9T Labs additive manufacturing machine [18]. 9T Labs offers a whole additive fusion technology including post treatment. The printing strategy is XY/Z with fiber direction along the Y-direction as drawn by the white line in Fig.1.

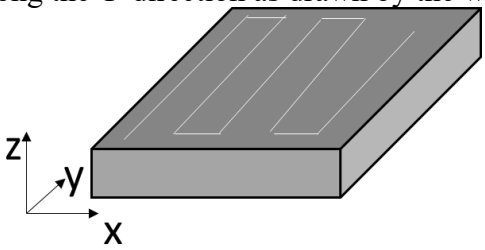

Fig. 1. Orientation of the printed plates with the building strategy (white line).

The material feedstock is a rectangular unidirectionnal carbon fiber pre-impregnated tape whose theoretical fiber volume fraction is 60 % [18]. The deposited tape contains a polyetherketoneketone (PEKK from Arkema company) matrix and AS4 carbon fiber. After printing, the parts are inserted into a mold, and a compression cycle is applied to densify the parts. This process guarantees high resistance complex shape parts. For the sake of clarity, the parts are 2- and 3-mm tick plates in this study. Three cases are compared i) Printed plate without consolidation (named UP), ii) Printed plates with a compression cycle at 334°C (CP-C1) and iii) Printed plates with a compression cycle at 360°C (CP-C2). The compression temperatures were chosen according to the thermal transitions of PEKK matrix. DSC (differential scanning calorimetry) were performed on about 10 mg of PEKK filament in aluminum pans with a Q200 TA Instruments DSC. The heating cycle is as follows: First heating ramp: 10°C.min^{-1} from 25°C to 380°C, cooling ramp: 10°C.min^{-1} from 380°C to 25°C, second heating ramp : 10°C.min^{-1} from 25°C to 380°C. Three samples were tested, only the second heating ramp of one sample is shown in Fig. 2. The filaments were dried at 140°C for 24h before testing. The glass transition is visible at 160°C, then the melting peak spreads from 300 to 360°C. The compression temperatures correspond to the maximum of the melting peak (334°C) and the end of the melting peak (360°C) for CP-C1 and CP-C2 respectively. The consolidation cycle is defined by a heating ramp at 15°C.min^{-1} under 30kN, an isothermal step at 334 or 360°C under 45kN for 180 s, followed by a cooling ramp at 7°C.min^{-1} under 45kN. Then, the parts are demolded when the temperature is below 160°C. The printing and post-treatment parameters are defined respectively in Table 1 and Table 2.

Table 1. Printing parameters.

Plate temperature (°C)	180
Chamber temperature (°C)	Inactive
Fiber Guide/Printing Temperature (°C)	360
Print speed (mm.min^{-1})	1000
Line width (mm)	0,9
Layer height (mm)	0,17

Table 2. Consolidation parameters.

	UP	CP-C1	CP-C2
Heating ramp (°C.min^{-1})	/	15	15
Isothermal Temperature (°C)	/	334	360
Max Pressure (kN)	/	45	45
Cooling ramp (°C.min^{-1})	/	7	7

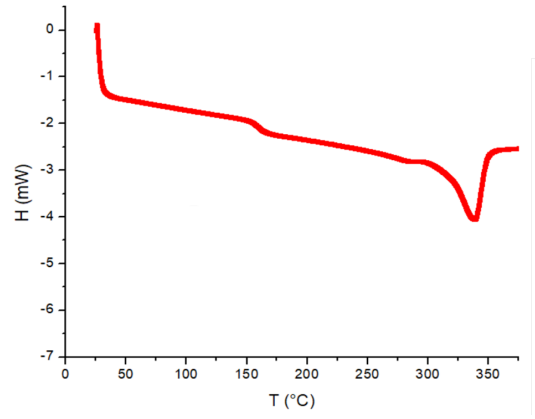

Fig. 2. DSC curve, second heating ramp for PEKK tape, 10°C.min^{-1}.

Methods

Before any characterization, all samples were dried at 140°C for 24h.

Short beam shear (SBS) tests were carried out on an Instron 4204 universal testing machine with a three-point bending device. The radius of the two supports and loading nose were 5 mm and 2 mm respectively, according to NF-EN 2463 standard. The cross-head speed was 1 mm.min^{-1}. For each configuration, at least three specimens were tested, the results were averaged. The strength of the SBS test was calculated from Eq. 1:

$$\tau_{SBS} = \frac{3}{4}\frac{P_{max}}{b.h} \quad (1)$$

with τ_{SBS} : Short-beam strength (SBS) (MPa), P_{max}: maximum load (N), b: sample width (mm), h: sample thickness (mm)
The sample density was measured by hydrostatic weighing in accordance with NF EN ISO 1183-1 standard. The density of the samples, ρ_s (g.cm^{-3}), was calculated by Eq. 2:

$$\rho_s = \frac{m_s}{(m_s - m_e)}\rho_{water} \quad (2)$$

with m_s : apparent mass of the sample in air (g), m_e : apparent mass of sample in water (g)
ρ_{eau} : water density
Then, the porosity was obtained by Eq. 3:

$$P = 1 - \frac{\rho_s}{\rho_f} \quad (3)$$

with ρ_f the density of the raw tape (according to the data sheet ρ_f= 1,58 g.cm^{-3}), ρ_s is the density of the sample and P is the porosity rate.

X-ray micro-computed tomography (µCT) was used to evaluate the porosity of the plates. Volume images were generated by a laboratory tomography device (Easytom RXSolution). The acquisition parameters were a tension of 150 kV and an intensity of 200 µA. 10 x 15 mm specimens were positioned on a rotation stage and 1440 projections of transmitted X-ray intensity field were recorded at each angular step of 0.25° by a flat panel detector (1920 x 1536 pixels) through an X-ray detector. Each projection was obtained by averaging ten images recorded at the same angular position. A volume image of the variations of the linear attenuation coefficient in the specimen was reconstructed from all radiographies by using a filtered back-projection algorithm. The distribution of grey levels in 3D images is due to local differences of density and so corresponds to a 3D representation of the microstructure of the specimen. Each volume image was reconstructed with the same voxel size of 13.48 µm. The pictures were treated with Avizo software. Each sample was divided into six parallelepipedic parts as seen in Fig. 3. The depth of the sample is not represented here but it is considered as well. Using a greyscale, a threshold is applied to separate the matrix and fiber part from the black part, i.e., the pores. The light grey part represents the clamping device used to hold the specimens: so, it is not considered for analysis. Furthermore, the air around the specimen is not counted as pores. The calculation of the global porosity rate is done by averaging the porosity rates of each zone.

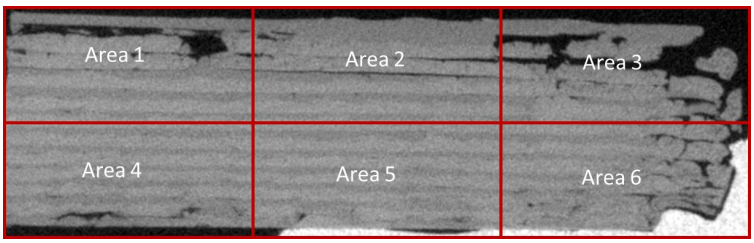

Fig. 3. Separations of area on XZ view.

Dynamic mechanical Analysis (DMA) was investigated using an ARES strain-controlled rheometer from TA Instruments in rectangular torsion mode. For dynamic analysis, sinusoidal strain γ* is imposed with a constant angular frequency ω. Viscoelasticity of polymers leads to a

phase lag between strain and stress σ* giving access to, in the linear viscoelastic domain, the complex dynamic modulus. Storage and loss moduli, G' and G'', were recorded as a function of temperature. Measurements were achieved from 25°C to 325°C with a 3°C.min^{-1} ramp. The angular frequency ω was 1 rad.s^{-1} and the strain γ was 0.1% for UP, 0.05% for CP-C1 and 0.1% for CP-C2 to stay within the linear viscoelastic domain. Sample sizes were 45 x 10 x 3 mm^3.

Results and discussions

Porosity.

Two different methods, hydrostatic weighing and micro-computed tomography were applied to evaluate the porosity. The results are presented in Fig. 4. The porosity for the reference plate (no consolidation) is 15% by tomography and 10% by hydrostatic weighing. The compression step at 334°C results in decreasing the porosity up to 3% by tomography and 7% by hydrostatic weighing. A higher compression temperature, 360°C, leads to a reduction of the porosity, below 1% whatever the technique. A high porosity is often reported for printed parts, for instance in the work by Tao et al. [4]. The compression step reduces the porosity. Indeed, the viscosity of the thermoplastic matrix decreases with temperature, resulting in easier polymer flow and closing of the pores. A representation of the theoretical structure of printed parts is schemed in Fig. 5.

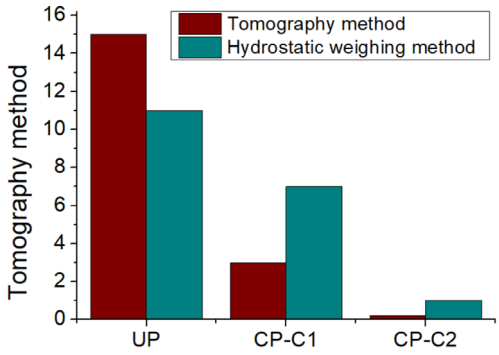

Fig. 4. Porosity for non-consolidated (UP), consolidated at 334°C (CP-C1), consolidated at 360°C (CP-C2) specimens.

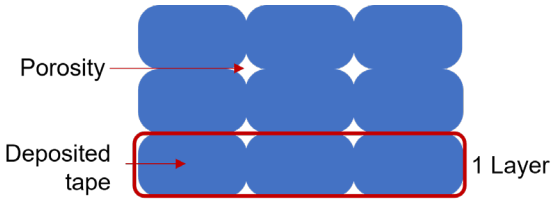

Fig. 5. Representation of the structure of a printing part (view XZ).

In the case of UP, besides pores presented in Fig. 5, delamination of the layers is observed. Indeed, the specimens were printed in a chamber without temperature control, resulting in low adhesion between tapes. Therefore, a higher porosity is measured on the specimen edges compared to the inner structure, as seen in Fig. 6. For the CP-C1 and CP-C2 plates, no delamination is detected by the software, leading to a better accuracy in the calculation of the porosity.

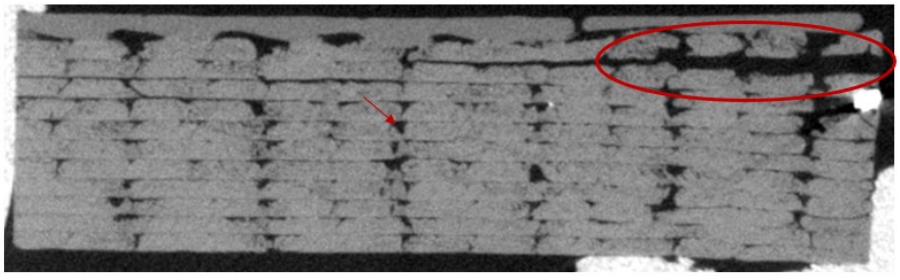

Fig. 6. XZ view of a slice of UP.

For the unconsolidated plate (UP), the porosity obtained by hydrostatic weighing is smaller than the one obtained from the density measurement. This is because external porosities due to

delamination are not considered in weighing, as water can seep into the narrowest pores on the sample edges.

For the consolidated specimens, the porosity is higher for hydrostatic weighing in both cases as seen in Fig. 4 for CP-C1 and CP-C2. The pores below 13,5 µm size (1 pixel) were not detected whereas hydrostatic weighing considers all pores whatever their sizes. A smaller pixel size would be necessary to detect smaller pores and to make both techniques to converge to the same porosity result. To sum up, CP-C2 has a much lower porosity than other specimens. The consolidation step at 360°C allows the PEKK matrix to flow more easily and to close the voids compared to 334°C. This temperature corresponds to the maximum of the melting peak. At this temperature, some crystalline lattices still remain, as a consequence, the viscosity is still too high to make the consolidation step effective.

Effect of compression on mechanical properties.

The results of SBS tests for unconsolidated specimens, compressed specimens at 334 and 360°C are shown in Fig.7a, b and C respectively. Interlaminar Shear Strength (ILSS) is defined by the first drops in stress on the curve. For UP, a more progressive and less brutal fall in stress is pointed out compared to the trend obtained for consolidated plates. ILSS results (calculated from the ISO 14130 standard) for the UP is 4,44$\pm$0,89 MPa whereas 42,54$\pm$2,36 MPa and 69,54$\pm$3,49 MPa were obtained for CP-C1 and CP-C2, respectively. The consolidation step has an impressive effect on ILSS with an increase of more than 800 % for CP-C1 and 1400 % for CP-C2. These results demonstrate the efficiency of the compression post-treatment after printing. A higher dispersion is noticed for UP whereas the curves for consolidated ones are closed one to each other. Moreover, increasing the temperature for the compression step increases the ILSS of about 40% when comparing CP-C2 and CP-C1. ILSS is related to interlayer adhesion. At 360°C, the viscosity is lower than at 334°C, giving more mobility to the macromolecules and a faster macromolecular diffusion across the layers. ILSS is mainly the contribution of two parameters: interlayer adhesion and porosity. We target to determine which one is the most influential on ILSS. For that, ILSS is plotted with the porosity in Fig.8. As expected, the ILSS value decreases with the increase in porosity. When the porosity tends towards zero, the ILSS value sharply increases. A hypothesis explaining such rise is related to the contact surface between tapes: Under pressure, the pore sizes decrease. Because of the elliptical shape of the tape section, this contact surface increases abruptly at the beginning and then slowly until the perfect contact between tapes is reached (flat surface). From a threshold, the effect of porosity is expected to be overlooked, giving a maximum ILSS value.

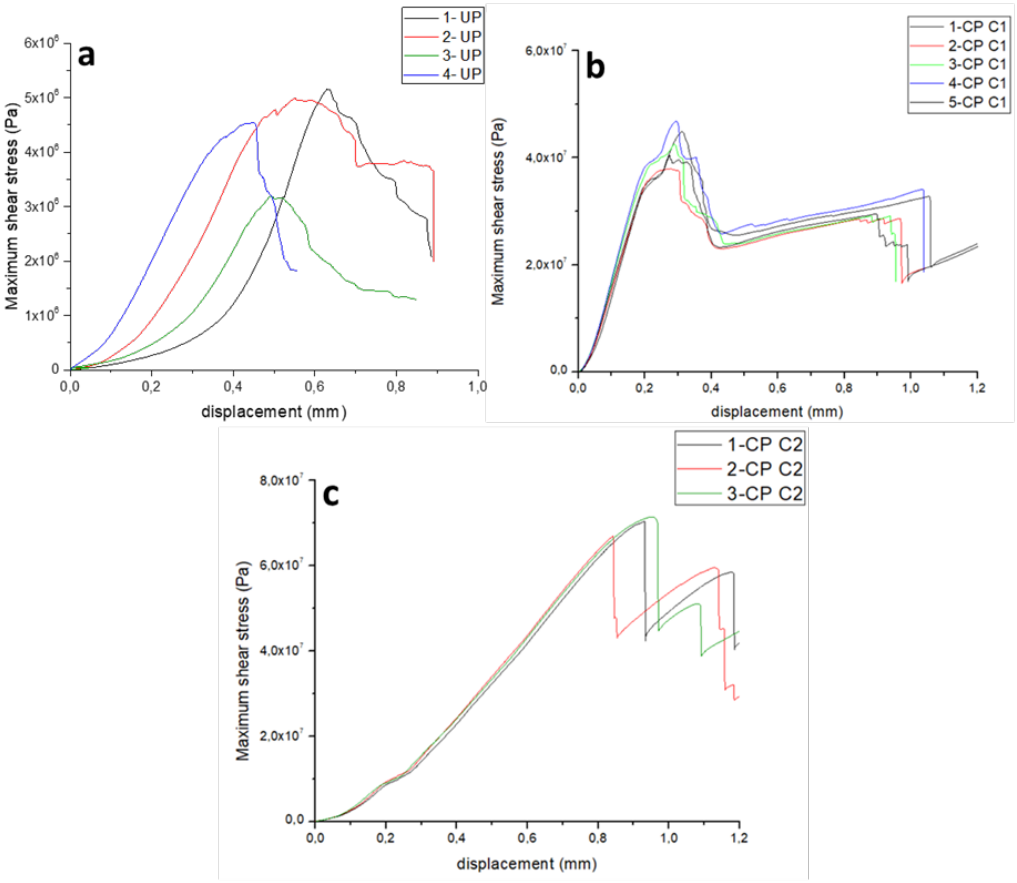

Fig. 7. SBS curves. a: plate UP ; b: plate CP-C1 ; c: plate CP-C2.

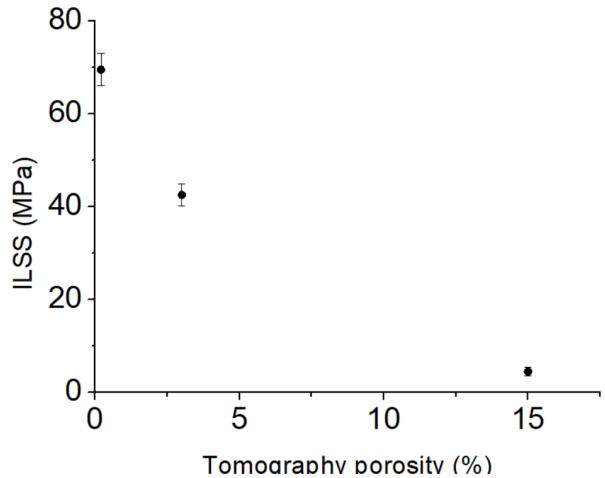

Fig. 8. Variation of SBS test results with porosity obtained by micro-computed. tomography

Effect of compression on dynamic moduli.

The dynamic moduli are presented in Fig. 9. In Fig. 9a, for all the specimens, a quasi-constant storage modulus G' is observed at the lowest temperatures up to 160°C, at this temperature, a sudden drop is associated to the glass transition (Tg). After the rubbery plateau, a last decrease towards 300°C corresponds to the softening of the amorphous phase of PEKK. As expected, G' for the unconsolidated plate is lower than for the consolidated ones. Surprisingly, the storage modulus in the glassy plateau is the highest for CP-C1. It means that the stiffness of the specimen consolidated at 334°C is higher than the one compressed at 360°C. Also, we notice a slight shift in the glass transition, around 170°C, with the lowest Tg for CP-C1. For the loss modulus G'' in Fig. 9b, a peak is observed at Tg and then a drop thereafter. The loss modulus (G'') is also higher in the case of CP-C1, which means that the material needs more energy to deform. In Fig.9c, the maximum of the ratio tan δ=G''/G' is shifted towards lower temperatures for CP-C1. This lower

Tg is associated with a higher macromolecular mobility in the amorphous phase. Also, this peak is broader and less symmetrical than the ones obtained for the UP and the plate consolidated at 360°C. This peak shape is often attributed to a higher polydispersity in chain lengths. In our case, it could stem from a higher dispersity in crystallite sizes. Indeed, in the case of compression at 334°C, the crystalline phase of the material has partially melted. This unmelted crystalline phase could hinder the crystallization during cooling, giving more time to the macromolecules to diffuse across the contact surface of the tapes. G' and G'' of CP-C1 are therefore higher than those of CP-C2. These results are supported by the degree of crystallinity results gathered in Table 3. The degree of crystallinity Xc is calculated from DSC curves with the Eq. 4:

$$Xc = \frac{\Delta Hf}{\Delta H_{100\%} * V_m} \quad (4)$$

With ΔHf the enthalpy of the melting peak of the first heating ramp, ΔH_(100%) the enthalpy of PEEK (considering the crystallinity of PEEK is close to those of PEKK) at 100% of crystallinity [19], V_m the volume fraction of matrix (0,4). Very high standard deviations of the degree of crystallinity are observed for UP and CP-C1 in Table 3 whereas those consolidated at 360°C are less disperse. This deviation indicates a non-homogeneity during crystallization. It means that the crystallization does not occur homogeneously within the part during consolidation at 334°C.

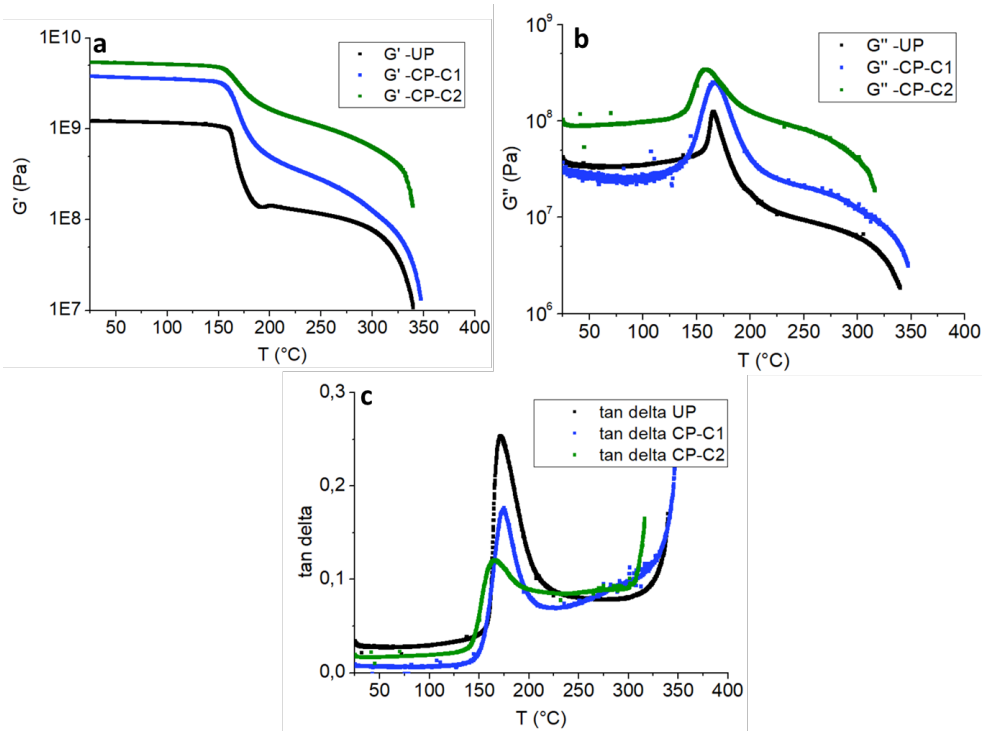

Fig. 9. DMA results for unconsolidated parts (UP), consolidated parts (CP) at 334°C (CP-C1) and 360°C (CP-C2): (a) storage modulus (G'); (b) loss modulus (G''), (c) tan δ.

Table 3. Degree of crystallinity of PEKK tapes and printed plates obtained from DSC curves

Material	Cristallinity (%)
PEKK	29 ± 3
UP	17 ± 2
CP-C1	17 ± 3
CP-C2	39 ± 15

Summary

To conclude, 9T Labs provides a complete additive manufacturing process to obtain printed parts with high mechanical strength. It consists of a printing step followed by a compression cycle. Two compression temperatures, 334 and 360°C were studied to determine the optimized conditions. When comparing to the reference plates (without the compression step), it reveals that the consolidation has a significant impact on part properties. The porosity was measured after printing on unconsolidated and consolidated parts by two techniques: tomography and hydrostatic weighing. The parts were characterized through short-beam strength tests, dynamic mechanical analysis, and differential scanning calorimetry. The aim was to compare the effect of the consolidation temperature at 334 and 360°C on porosity, ILSS and dynamic moduli.

The porosity was considerably reduced when the parts underwent consolidation post-treatment, the lowest porosity was obtained at 360°C, less than 1%, due to the PEKK matrix which is fully melted at this temperature. ILSS was initially near 4 MPa for the non-consolidated plates, whereas for those consolidated at 334°C and 360°C, ILSS were 42 and 69 MPa respectively. This result is higher than the ones found by Van Der Varken et al. [17]. This higher strength could stem from the reduction of porosity and increase of contact surface. ILSS results are clearly related with porosity, but the trend is not linear, indication the contribution of other phenomena such as macromolecular orientation. The highest storage modulus was obtained for the part consolidated at 334°C. A hypothesis could be linked to chains conformation: they are oriented in the extrusion direction whereas this organization is lost at 360°C. The loss factor (tan $\boldsymbol{\delta}$) indicates a lower glass transition for the part consolidated at 334°C. This lower glass transition is consistent with a higher macromolecular mobility in the amorphous phase and a lower degree of crystallinity. Further works will focus on understanding the effect of thermal cycles on crystal morphology and the role of crystallinity on interfilament adhesion.

References

[1] N. Shahrubudin, T.C. Lee, R. Ramlan, An Overview on 3D Printing Technology: Technological, Materials, and Applications, Procedia Manuf. 35 (2019) 1286-1296. https://doi.org/10.1016/j.promfg.2019.06.089

[2] G.W. Melenka, B.K.O. Cheung, J.S. Schofield, M.R. Dawson, J.P. Carey, Evaluation and prediction of the tensile properties of continuous fiber-reinforced 3D printed structures, Compos. Struct. 153 (2016) 866-875. https://doi.org/10.1016/j.compstruct.2016.07.018

[3] B. Brenken, E. Barocio, A. Favaloro, V. Kunc, R.B. Pipes, Fused filament fabrication of fiber-reinforced polymers: A review, Addit. Manuf. 21 (2018) 1-16. https://doi.org/10.1016/j.addma.2018.01.002

[4] Y. Tao, F. Kong, Z. Li, J. Zhang, X. Zhao, Q. Yin, D. Xing, P. Li, A review on voids of 3D printed parts by fused filament fabrication, J. Mater. Res. Technol. 15 (2021) 4860-4879. https://doi.org/10.1016/j.jmrt.2021.10.108

[5] L.M. Maloo, S.H. Toshniwal, A. Reche, P. Paul, M.B. Wanjari, A Sneak Peek Toward Polyaryletherketone (PAEK) Polymer: A Review, Cureus. 14 (2022). https://doi.org/10.7759/cureus.31042

[6] H. Pérez-Martín, P. Mackenzie, A. Baidak, C.M. Ó Brádaigh, D. Ray, Crystallinity studies of PEKK and carbon fibre/PEKK composites: A review, Compos. Part B Eng. 223 (2021) 109127. https://doi.org/10.1016/j.compositesb.2021.109127
[7] Y. Wang, W.-D. Müller, A. Rumjahn, F. Schmidt, A.D. Schwitalla, Mechanical properties of fused filament fabricated PEEK for biomedical applications depending on additive manufacturing parameters, J. Mech. Behav. Biomed. Mater. 115 (2021) 104250. https://doi.org/10.1016/j.jmbbm.2020.104250
[8] A.D. Schwitalla, T. Spintig, I. Kallage, W.-D. Müller, Flexural behavior of PEEK materials for dental application, Dent. Mater. 31 (2015) 1377-1384. https://doi.org/10.1016/j.dental.2015.08.151.
[9] R. Davies, N. Yi, P. McCutchion, O. Ghita, Mechanical property variance amongst vertical fused filament fabricated specimens via four different printing methods, Polym. Int. 70 (2021) 1073-1079. https://doi.org/10.1002/pi.6172
[10] K.M. Rahman, T. Letcher, R. Reese, Mechanical Properties of Additively Manufactured PEEK Components Using Fused Filament Fabrication, in: American Society of Mechanical Engineers Digital Collection, 2016. https://doi.org/10.1115/IMECE2015-52209
[11] D. Veazey, T. Hsu, E.D. Gomez, Next generation high-performance carbon fiber thermoplastic composites based on polyaryletherketones, J. Appl. Polym. Sci. 134 (2017). https://doi.org/10.1002/app.44441
[12] F. Ning, W. Cong, J. Qiu, J. Wei, S. Wang, Additive manufacturing of carbon fiber reinforced thermoplastic composites using fused deposition modeling, Compos. Part B Eng. 80 (2015) 369-378. https://doi.org/10.1016/j.compositesb.2015.06.013
[13] N. van de Werken, H. Tekinalp, P. Khanbolouki, S. Ozcan, A. Williams, M. Tehrani, Additively manufactured carbon fiber-reinforced composites: State of the art and perspective, Addit. Manuf. 31 (2020) 100962. https://doi.org/10.1016/j.addma.2019.100962
[14] D. Garcia-Gonzalez, M. Rodriguez-Millan, A. Rusinek, A. Arias, Investigation of mechanical impact behavior of short carbon-fiber-reinforced PEEK composites, Compos. Struct. 133 (2015) 1116-1126. https://doi.org/10.1016/j.compstruct.2015.08.028
[15] P. Wang, B. Zou, S. Ding, L. Li, C. Huang, Effects of FDM-3D printing parameters on mechanical properties and microstructure of CF/PEEK and GF/PEEK, Chin. J. Aeronaut. 34 (2021) 236-246. https://doi.org/10.1016/j.cja.2020.05.040
[16] M. Luo, X. Tian, J. Shang, W. Zhu, D. Li, Y. Qin, Impregnation and interlayer bonding behaviours of 3D-printed continuous carbon-fiber-reinforced poly-ether-ether-ketone composites, Compos. Part Appl. Sci. Manuf. 121 (2019) 130-138. https://doi.org/10.1016/j.compositesa.2019.03.020
[17] N. van de Werken, P. Koirala, J. Ghorbani, D. Doyle, M. Tehrani, Investigating the hot isostatic pressing of an additively manufactured continuous carbon fiber reinforced PEEK composite, Addit. Manuf. 37 (2021) 101634. https://doi.org/10.1016/j.addma.2020.101634
[18] Solutions Manufacture strong, lightweight, sustainable products like never before 9t Labs, https://www.9tlabs.com/solutions/additive-fusion-solution (accessed December 7, 2022).
[19] M. Doumeng, L. Makhlouf, F. Berthet, O. Marsan, K. Delbé, J. Denape, F. Chabert, A comparative study of the crystallinity of polyetheretherketone by using density, DSC, XRD, and Raman spectroscopy techniques, Polym. Test. 93 (2021) 106878. https://doi.org/10.1016/j.polymertesting.2020.106878